Vietnam Journal of Earth Sciences, 48(3), 393−407, https://doi.org/10.15625/2615-9783/24406

Vietnam Journal of Earth Sciences
https://vjs.ac.vn/index.php/jse

Shrinkage curve and its role in estimating unsaturated shear strength and permeability functions for a weathered soil

Thi Phuong An Tran*[1], Delwyn G. Fredlund[2], Do Quang Thien[1]

[1]*University of Sciences, Hue University, Hue City, Vietnam*
[2]*University of Saskatchewan, Saskatoon, Saskatchewan, Canada*

Received 31 January 2025; Received in revised form 13 January 2026; Accepted 30 March 2026

ABSTRACT

The soil shrinkage curve (SC) and the shrinkage limit are important for assessing the impact of volume change as soil dries. The SC is used to calculate the degree of saturation from the soil-water characteristic curve (*S*-SWCC) and is subsequently used to estimate other unsaturated soil property functions, such as shear strength and hydraulic conductivity. The present research aims are to: (1) identify the most appropriate parameters for the estimation for the SC without conducting a SC test, (2) investigate the effect of the initial compaction degree, characterized by void ratio and dry density, on the SC, and (3) emphasize the role of SC as it relates to the unsaturated shear strength and permeability functions. To achieve these objectives, the SC and SWCC tests were conducted on a weathered soil sample collected from a natural landslide slope along Route 74 connecting A Luoi and Nam Dong in Hue, Vietnam. The findings show that the SC can be predicted using empirical equations, thereby negating the need for direct SC testing. Unsaturated soil functions can be estimated from the SC and *S*-SWCC.

Keywords: Shrinkage curve, shrinkage limit, soil-water characteristic curve, unsaturated soil functions.

1. Introduction

In geotechnical and geo-environmental engineering practice, the changes in soil suction and degree of saturation are critical for predicting slope stability (Dao et al., 2023; Phạm et al., 2023; Tran et al., 2023a). The relationship between the degree of saturation and suction within the soil is fundamentally defined by the soil-water characteristic curve (SWCC).

The SWCC can be categorized into three primary families of curves based on water variables used: gravimetric water content (*w*-SWCC), volumetric water content (θ-SWCC, and degree of saturation (*S*-SWCC) (Fredlund et al., 2012). The *S*-SWCC accounts for soil volume changes and is commonly used to compute unsaturated soil functions, whereas the *w*-SWCC is most often measured in the laboratory. Therefore, the SC, which presents the change in void ratio with changes in gravimetric water content (i.e., mass water content) (Haines, 1923), is introduced. The SC can be combined with the *w*-SWCC to account for volume change and obtain the *S*-SWCC. In the process, the *S*-SWCC can be used to determine the soil's true air-entry value. Each SWCC family exhibits hysteresis, with a drying curve for water loss and a wetting curve for water gain.

*Corresponding author, Email: ttphuongan@hueuni.edu.vn

This study focuses solely on the drying *w*-SWCC, assuming negligible hysteresis between the drying and wetting curves.

Three types of SCs have been defined based on linear and curved line segments (Leong and Wijaya, 2015). In this study, the SC is defined by two linear segments (i.e., numbered 1 and 2) and a curved segment, as shown in Fig. 1. The 1-linear segment defines the decrease in water content during the initial stages of drying. The number 2-linear segment defines the drying curve in the zero-shrinkage line. The soil remains near-saturated during the initial stages of drying, even as the water content decreases, and then follows a curved path of residual shrinkage until it reaches the zero-shrinkage line. The point where the fully-saturated line intersects the extended zero-shrinkage line is commonly referred to as the shrinkage limit (Wijaya and Leong, 2016).

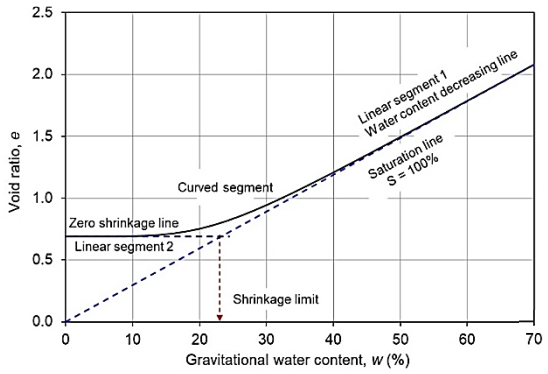

Figure 1. Typical 2-linear SC (Modified after (Fredlund et al., 2002; Leong and Wijaya, 2015))

Numerous researchers have introduced a variety of mathematical functions, such as a polynomial function (Giráldez et al., 1983; Tariq and Durnford, 1993), a hyperbola function (Fredlund, 2000), a logistic function (Peng and Horn, 2007), and a single continuous function (Leong and Wijaya, 2015). This study uses the hyperbolic equation proposed by Fredlund (2000) to predict SC (Eq. [1]). The hyperbola equation appears to provide excellent fits to measured data for most soils prepared under near-saturated conditions (Fredlund, 2019).

$$e(w) = a_{sh}[(\frac{w}{b_{sh}})^{c_{sh}} + 1]^{1/c_{sh}} \quad [1]$$

where a_{sh} is the minimum void ratio (e_{min}) upon complete drying; b_{sh} is related to the slope of the zero-shrinkage line; w is gravimetric water content, and c_{sh} is the variable related to the sharpness of the SC.

The a_{sh}-fitting parameter in the equation used by Fredlund (2000) is related to the soil's SL by Eq. [2].

$$a_{sh} = SL \times G_s \quad [2]$$

where G_s is the specific gravity of the soil. The *SL* is the amount of water required to fill the soil voids if the soil is dried to its minimum.

The b_{sh} fitting parameter of the SC equation can be calculated from Eq. [3].

$$b_{sh} = a_{sh}S_o/G_S \quad [3]$$

where S_o is the initial degree of saturation of the soil.

There was a close fit between the c_{sh} fitting parameter measured on SCs and the plasticity ratio (i.e., Plastic limit (*PL*) / Liquid limit (*LL*)) of soils (Wong et al., 2019).

$$c_{sh} = 1.7 + e^{3.1^{PL/LL}} \quad [4]$$

where *e* is the Euler number, equal to 2.7183.

The SC can also be estimated with sufficient accuracy in most situations using plasticity classification properties (Holtz et al., 1981). The *SL* can be defined on the Casagrande Plasticity Chart (Casagrande, 1932), along with the basic classification properties (G_s, *PL*, *LL,* and plastic index *PI*). The fitting parameters for the Fredlund (2000) SC equation (i.e., a_{sh}, b_{sh}, c_{sh}) can then be predicted. As a result, the SC curve can be predicted without the need for direct testing.

The study evaluates two approaches for predicting the SC. One approach uses the SL obtained from the plasticity chart and the aforementioned empirical equations (i.e., Eqs. [1], [2], [3], and [4]) to predict the SC parameters. The other method uses the minimum void ratio along with Eqs. [1], [2],

[3], and [4] to determine the SC parameters. The predicted results are compared to the experimental SC data and the best-fitting curve (Eq. [1]). Furthermore, the study examines the influence of compaction degree, as measured by the target initial void ratio and dry density, on the obtained SC. Additionally, the study emphasizes the change in the "apparent" air-entry value when the SC is combined with *w*-SWCC to define the *S*-SWCC. The *S*-SWCC is then used to predict the unsaturated soil's shear strength and permeability functions. To achieve the study's objective, SC and SWCC tests are conducted on weathered soil. The soil was sampled in a disturbed state from a natural landslide slope along Route 74 in A Luoi, Hue, where the weathered crust section is clearly exposed. The area is frequently subjected to various natural hazards, particularly storms and landslides.

2. Materials and Experiment Procedure

2.1. Soil material

The disturbed soil sample was taken from a slope along the Route 74 connecting A Luoi to Nam Dong in Hue, Vietnam (16°06’59’’N, 107°24’54’’E). The slope is 3 meters in height and extends over an area of approximately 200 m^2. The soil is the weathered product of granite with gneissic structures belonging to the Dai Loc complex. The soil is dark yellow to reddish brown (Fig. 2).

Figure 2. Taking sample from the field (16°06'59"N, 107°24'54"E)

The soil sample was thoroughly air-dried at room temperature. The resulting clods were gently broken apart in a mortar using a rubber-covered pestle (ASTM D421). Laboratory data show that the soil contains 46.20% sand, 49.12% silt, and 2.68% clay (ASTM-D6913, 2009) (Fig. 3). The soil has a *LL* of 26.35 % and a *PL* of 19.05% (ASTM-D4318, 2017). The soil can be classified as silty clay with sand, *ML-CL* (ASTM-D2487, 2025). The G_s of the soil were measured as 2.65 (ASTM D854).

Before the SC and *w*-SWCC tests, the soil sample was dried in the oven at 105°C until a constant mass was achieved. The dried soil was then passed through a No. 10 sieve (2 mm opening). Particles passing through the sieve were collected and used for preparing the SC and *w*-SWCC test specimens.

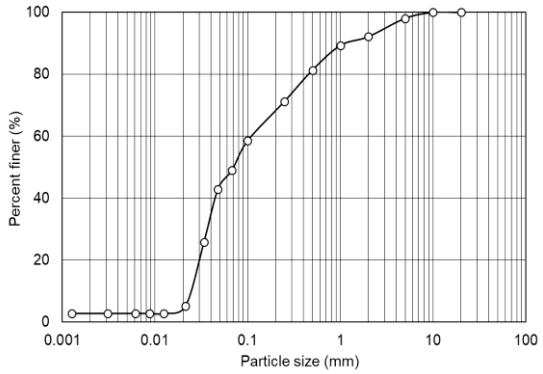

Figure 3. Grain size distribution of soil

2.2. Experiment procedures

2.2.1. w-SWCC

Specimen preparation

To conduct the *w*-SWCC test (ASTM-D6836, 2016), the procedures followed the standard except that the SWC-050 testing equipment and protocols (GSCT, 2022) were used. The remolded soil specimen was prepared within a holding ring with a 6.3 cm diameter and placed in contact with the ceramic high-air-entry disk. The soil was placed into the ring in several layers. Each layer was lightly tapped on the surface to remove voids and achieve a uniform density. The dry density of the soil specimen was 1.2 g/cm^3.

Saturation process

Tap water was added outside the ring and at the base of the specimen cell to allow water to infiltrate upward into the soil, facilitating the removal of air bubbles. The specimen was left to saturate for more than 2 days, until water appeared at its surface, indicating it had reached full saturation. The physical properties of the remolded soil specimen at dry and saturation conditions were summarized in Table 1 (see Appx.).

Experimental procedure

Pneumatic pressure was applied in increments of 1, 3, 5, 10, 20, 50, 100, 200, and 400 kPa. Each pressure was applied continuously for 72 hours to the soil. Water was released from the specimen through the ceramic disk and then via drainage holes. At the end of each pressure stage, the water adhering to the base was wiped away with an absorbent cloth. The cell with the specimen was then weighed again. The difference in weight is the weight of water moved from the soil specimen under the applied pressure increment.

The setup in the pressure plate cell included the dead loads, porous stone, and soil specimen (Fig. 4). The purpose of these dead loads is to ensure sufficient hydraulic contact between the water phase and the soil specimen and the high air-entry disk, and to ensure that the linear variable differential transformer (LVDT) is within its measurement range. In this study, the vertical displacement data recorded by the LVDT are not included.

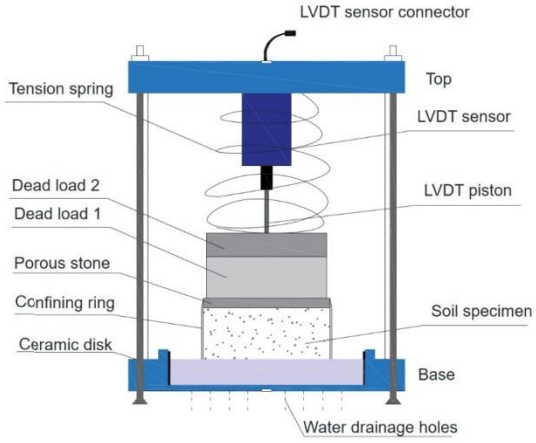

Figure 4. Schematic diagram of the soil specimen and pressure plate cell (Tran et al., 2023c)

It should also be noted that water drainage through the holes in the base plate provides a lower-boundary pore-water pressure condition, since drainage occurs against atmospheric air pressure. Therefore, the average negative pore-water pressure in the soil specimen is 0.318 kPa (Tran et al., 2023c). Since the soil is subjected to the token

load of 2.38 kPa, the initial soil suction will be (2.38–0.318) = 2.06 kPa. Therefore, the initial gravimetric water content measurement for the SWCC would yield the water content corresponding to a suction of 2.06 kPa.

Several specimens were initially prepared and tested, but only one specimen satisfying all verification criteria was used to present the *w*-SWCC. This ensures the reliability of the reported results.

2.2.2. SC *test*

Specimen preparation

The remolded soil specimen was prepared within a holding ring with a 4.8 cm diameter and a 2.2 cm height. The target density was approximately 1.2 g/cm^3 to ensure consistency with the soil specimen's dry density used in the *w*-SWCC test. Matching the target dry density or void ratio is essential to reliably integrate the *w*-SWCC data with the SC analysis for the same soil specimen.

In this study, to examine the effect of compaction degree, represented by void ratio and dry density, on SC, two additional target states were considered: one with a dry density higher than 1.2 g/cm^3 and the other with a lower value. The target densities (γ_{ct}) were achieved by compacting the soil within the ring layer by layer. The specimens, arranged from the highest to the lowest dry density, are referred to as Case 1, Case 2, and Case 3 in this study. The target initial void ratio of the remolded specimen was denoted as e_{ot}.

Saturation process

The specimen is placed on a porous stone covered with filter paper, and is placed in a container. The container was filled with tap water reaching the halfway point of the soil specimen. Saturation took more than 2 days, during which the water appeared at the surface of the specimen.

Experimental procedure

The saturated specimen was left at room temperature for natural drying. Changes in mass, diameter, and height of the specimen were recorded (Fig. 5). Changes in mass were converted to changes in water content, while changes in diameter and height were used to calculate the soil void ratio (Fredlund et al., 2012).

Figure 5. Measuring the diameter of the SC specimen

2.3. Methods of Analysis

2.3.1. w-SWCC

The mathematical equation introduced by Fredlund and Xing (1994) was used and applied to the *w*-SWCC (Fredlund and Xing, 1994):

$$w(\psi) = \frac{w_o C(\psi)}{\left(\ln\left(\exp(1) + \left(\psi/a_{fx}\right)^{n_{fx}}\right)\right)^{m_{fx}}} \quad [5]$$

where: $w(\psi)$ = gravimetric water as a function of soil suction; w_o = initial gravimetric water, which is also called mass water content and is measured as the ratio of water in a soil specimen to the mass of dry soil ψ = soil-suction; ψ_r = residual suction; a_{fx} = fitting parameter related primarily to the inflection point; n_{fx} = fitting parameter related primarily to the slope of the function; m_{fx} = third fitting parameter related primarily to the residual point; and $C(\psi)$ = Correction function applied in the high suction range and ending at a

suction of one million kPa. The Correction, $C(\psi)$The function is shown in Eq.[6]

$$C(\psi) = 1 - \frac{\ln(1 + {}^{\psi}/_{\psi_r})}{\ln(1 + {}^{10^6}/_{\psi_r})} \quad [6]$$

A sigmoidal equation can be applied to both the *w*-SWCC and the *S*-SWCC (Fredlund and Xing, 1994).

In this study, the air-entry value obtained from the *w*-SWCC is denoted as *gev*, while that obtained from the *S*-SWCC is denoted as *AEV*.

2.3.2. Shrinkage Curve

The SC equation for gravimetric water content versus void ratio (Fredlund, 2000) used in this study is given by Eq. [1].

The degree of saturation was subsequently expressed as a function of gravimetric water content and void ratio.

$$S(w) = \frac{w(\psi)G_s}{e(w)} \quad [7]$$

where $w(\psi)$ is the gravimetric water content as a function of soil suction, and $e(w)$ is the void ratio written as a function of gravimetric water content.

The parameters obtained from *S*-SWCC were denoted as a'_{fx}, n'_{fx}, and m'_{fx} in this study.

2.3.3. Shrinkage Limit, SL, from Casagrande's plasticity chart

The A-line and the U-line for soils were found to have a common origin defined by an *x*-coordinate (i.e., a fictitious *LL*) of -43.5 and a *y*-coordinate (i.e., a fictitious *PI*) of -46.5 (Fig. 6). For example, a soil with LL_A and PI_A is shown as point A on the plasticity chart. If a line is drawn from point A to the converged point of the A-line and U-line, the intersection points with the x-coordinate (i.e., *LL* line) indicate a shrinkage limit *SL* of the soil.

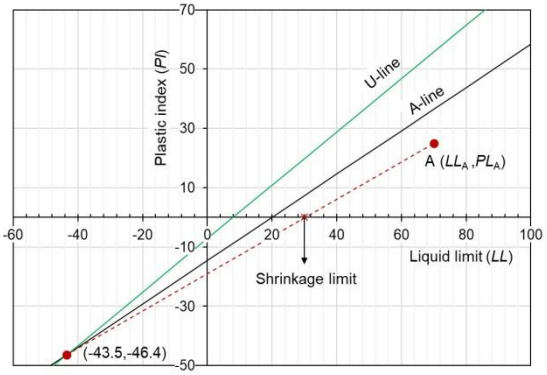

Figure 6. Obtaining *SL* from Casagrande's plasticity chart (Casagrande, 1932)

2.3.4. Methods of estimating SC

To identify the most suitable methods for predicting SC based on plasticity properties and Eq. [1] without performing an actual SC test, two methods for estimating the SC parameters were examined. The results were verified with the experimental data referred to as Method 1.

Method 1: SC experiment calibration

An actual SC test was conducted, with the experimental data subsequently fitted using Eq. [1]. This result serves as a reference for verifying predictions from the other methods. The shrinkage limit was obtained from the SC and denoted as *SL*. The value of *SL* is obtained by projecting the intersection point of the SC and saturation line onto the gravimetric water content axis. Furthermore, by rearranging Eq. [2], the shrinkage limit was also calculated as $SL_{ash} = a_{sh} / G_s$

Method 2: SC from the e_{min} approach

The a_{sh} is defined as e_{min} upon complete drying. The idea of this method is to estimate the SC from the e_{min} of the specimen. e_{min} was obtained by oven-drying until no volume changes were found. b_{sh} and c_{sh} were then obtained using Eqs. [3] and [4]. The fitting SC was constructed by applying Eq. [1], and the shrinkage limit obtained from the estimated

SC was called SL_{emin}. The shrinkage limit was also calculated by using the rearranged form of Eq. [2], $SL_{ash\text{-}emin} = a_{sh} / G_s$.

Method 3: Estimated SC from shrinkage limit on Plasticity Chart

This method illustrates how the shrinkage limit obtained using Casagrande's Plasticity Chart is applied for SC prediction. In this study, the shrinkage limit obtained on the Plasticity Chart was denoted as SL_{Cas}. The SL_{Cas} obtained were used to calculate a_{sh} (Eq. [2]). b_{sh} and c_{sh} were obtained by Eqs. [3] and [4]. a_{sh}, $b_{sh,}$ and c_{sh} parameters were substituted into Eq. [1] to generate the predicted SC.

2.3.5. Unsaturated Shear Strength equation

Many equations have been proposed to predict the unsaturated shear strength function of soil (Bao et al., 1998; Fredlund, 2019; Fredlund et al., 1995; Khalili and Khabbaz, 1998; Vanapalli, 2009; Vanapalli et al., 1996). Figure 7 illustrates the typical shapes of the measured unsaturated shear strength envelope. The shear strength envelope begins to curve once the soil's air-entry value is exceeded. The shear strength envelope progressively bends and becomes nearly horizontal as the soil approaches residual suction conditions (Tran et al., 2023b; Vanapalli and Oh, 2021; Zhang et al., 2014).

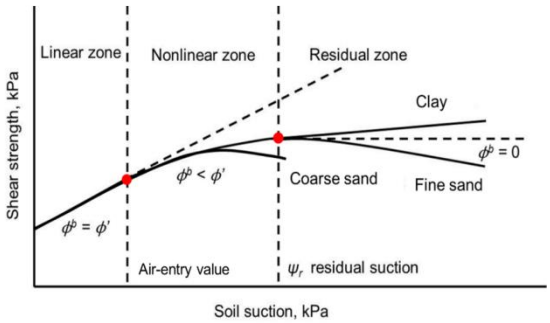

Figure 7. Typical shapes of measured unsaturated shear strength envelopes (Tran et al., 2023b; Vanapalli and Oh, 2021; Zhang et al., 2014)

In this study, the equation proposed by Fredlund (2019) was applied without examining the strengths and weaknesses of other equations. The equation applied the ζ coefficient suggested by Bao et al., 1998).

Bao et al. (1998) proposed an unsaturated shear strength equation that introduced a parameter.

$$c = c' + (u_a - u_w)[\zeta] tan\phi' \quad [8]$$

$$\zeta = \frac{log(u_a - u_w)_r - log(u_a - u_w)}{log(u_a - u_w)_r - log(u_a - u_w)_b} \quad [9]$$

where u_a is pore-air pressure, u_w is pore-water pressure, $(u_a - u_w)_r$ is residual suction, and $(u_a - u_w)_b$ is the air-entry value. The value is defined as a normalized logarithmic function of matric suction $(u_a - u_w)$, bounded by the residual suction $(u_a - u_w)_r$ and the air-entry value $(u_a - u_w)_b$, and it ranges from 0 to 1 on a logarithmic scale. The ζ value is 1.0 at the *aev* and decreases to a value of zero at residual suction conditions (Bao et al., 1998).

Fredlund (2019) used the ζ coefficient to define the slope of the shear strength function rather than the actual shear strength (Fredlund, 2019)

For suction ≤ air-entry value:

$$c_{i=0} = c_{aev} = c' + (u_a - u_w)_b tan\phi' \quad [10]$$

$$(u_a - u_w)_{i=0} = (u_a - u_w)_b \quad [11]$$

For suction > air-entry value:

$$c_{i+1} = [(u_a - u_w)_{i+1} - (u_a - u_w)_i][\zeta] + c_i \quad [12]$$

where ζ is the coefficient suggested by Bao et al. (1998) and $(u_a - u_w)_b \leq (u_a - u_w)_i \leq (u_a - u_w)_r$, i ≥ 0, and i indicates step-wise integration between the air-entry value and residual suction (Fredlund, 2019).

In this study, the effective cohesion of soil was assumed as 4 kPa, and the effective friction angle of soil was calculated as 32.45° using the empirical equation proposed by Salih 2012 (Salih, 2012)

$$\varphi' = 0.14\ (234.5 - \%\ \text{clay-size particles}) \quad [13]$$

2.3.6. Unsaturated permeability function

Accurate permeability prediction is fundamental to the reliability of flow

simulations (Hoang et al., 2024). Numerous permeability equations have been proposed based on SWCC features to predict unsaturated permeability of soils (Brooks and Corey, 1964; Fredlund et al., 1994; Gardner, 1958; van Genuchten, 1980). This study does not aim to compare these equations; rather, it emphasizes the role of the *AEV* obtained from the *S*-SWCC. Accordingly, the equation proposed by Fredlund et al (1994) was adopted in this study (Fredlund et al., 1994)

$$k_r(S_l) = \sum_{j=l}^{m} \frac{2(j-l)+1}{\psi_j^2} \Big/ \sum_{j=l}^{m} \frac{2j-1}{\psi_j^2} \quad [14]$$

where:

l = interval number that increases with decreasing degree of saturation,

m = total number of intervals between the saturated degree of saturation and the lowest water content on the *S*-SWCC,

j = interval counter, where $j = l, \ldots, m$,

ψ_j = soil suction corresponding to the mid-point of the j^{th} interval.

3. Experimental Results and Analysis

3.1. Effects of target initial void ratio on SCs

Figure 8 presents the different SC results for three cases of e_{ot}. The experimental shrinkage data of the soil followed the 2-linear SC. For this observation, the experimental data were then fitted using Eq. [1]. The different e_{ot} values prepared show different e_{min}, SC parameters a_{sh}, b_{sh}, c_{sh}, and *SL* obtained as the SC tests were completed (Fig. 8). Under each e_{ot} condition, e_{min} and a_{sh} showed comparable values, which further confirms that the a_{sh} parameter of SC is appropriately defined as being equivalent to e_{min}.

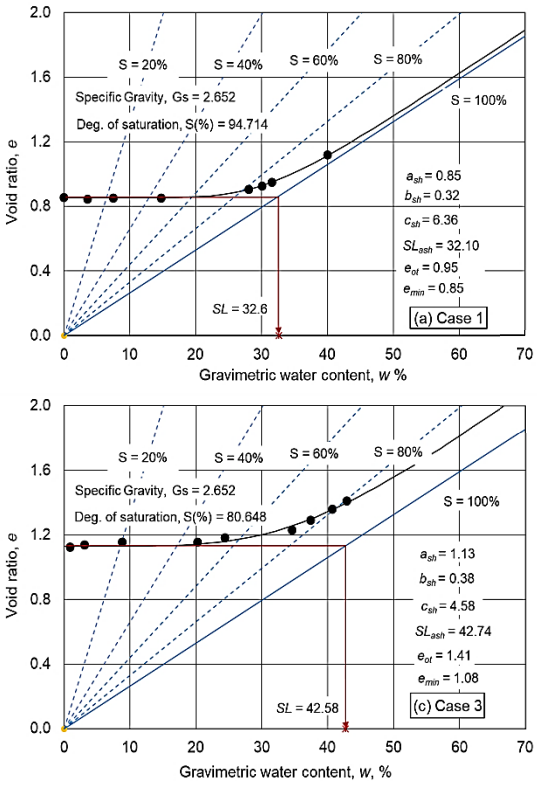

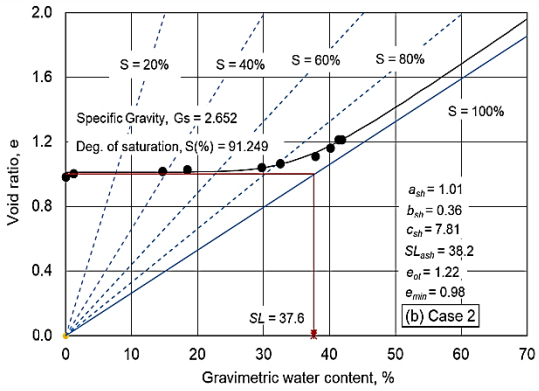

Figure 8. SCs and related parameters for compacted soil with e_o (a) 0.951; (b) 1.216 and (c) 1.410

Figure 9 presents the shrinkage-fitting curves for each case. It is shown that the curve shifts slightly upward with e_{ot} values. The e_{min} observed at the end of the SC test had a

proportional change with the e_{ot} (Fig. 10). e_{min} increased from 0.85 to 1.08 as e_{ot} varied from 0.95 to 1.41. The linear relationship exhibited a relatively steep slope (Fig. 10), indicating that e_{min} was highly sensitive to changes in e_{ot}. A small increase in e_{ot} led to a relatively large increase in e_{min}.

The *SL* and SL_{sh} values demonstrated a close correspondence (Fig. 8). As the e_{ot} affected e_{min}, the *SL* values obtained from SCs also changed with e_{ot} and γ_t. A decrease in γ_t from 1.36 g/cm^3 to 1.1 g/cm^3 was accompanied by a linear increase in *SL* from 32.6 % to 42.6%. Meanwhile, *SL* decreased linearly with increasing e_{ot} from 0.95 to 1.41 (Fig. 11). The contrasting trends of *SL* with respect to e_{ot} and γ_t reflected the fundamental physical characteristics of soil, whereby higher e_{ot} values correspond to lower γ_t.

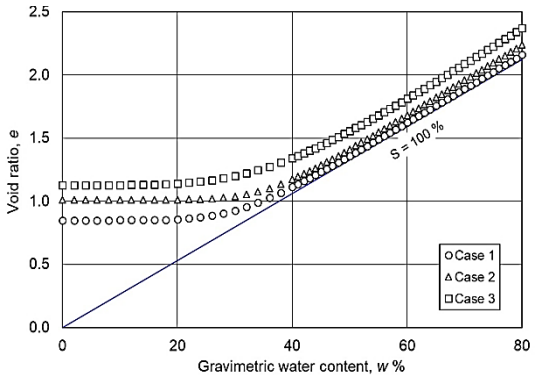

Figure 9. Changes in SC with initial void ratio

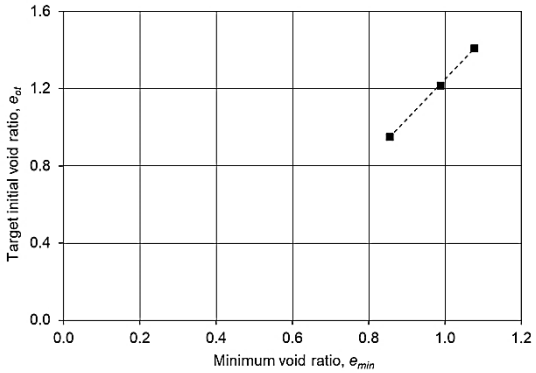

Figure 10. Changes the minimum void ratio with the initial void ratio

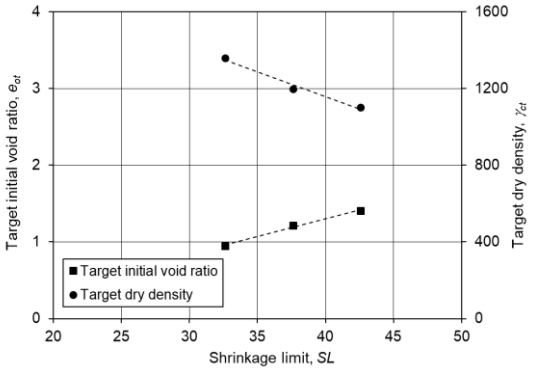

Figure 11. Changes of *SL* with initial compaction conditions

3.2. SC result for different approaching methods

Methods 1 and 2 produced the best-fitting curves. In contrast, the curve generated by Method 3 showed poor alignment with the experimental data along the zero-shrinkage line (Fig. 12). Both the e_{min} and the zero-shrinkage line obtained from Method 3 were lower compared to those from Methods 1 and 2 (Fig. 12), which explained the lower SL_{Cas} value of 17.50 reported for Method 3 (Table 2, see Appx.).

Method 2 used the soil specimen's e_{min} to define a_{sh}, which closely matched the value obtained by Method 1. Therefore, the zero-shrinkage lines of the two methods were nearly identical. The observed discrepancy arose from differences in shrinkage curvatures and loading lines, primarily due to differences in c_{sh}. Calculating c_{sh} based on its relationship to *PL* and *LL* can lead to errors. However, this gap can be acceptable for predicting the SC without requiring a direct SC test.

For Method 3, all SC parameters were obtained from the experimental *PL* and *LL*, both directly and indirectly. The method began by using the SL_{Cas} from the plasticity chart to back-calculate SC parameters, which may lead to errors in constructing the shrinkage-fitting curve. In other words, using the plasticity chart did not provide the correct

SL of the soil. It should be noted that this observation was based on a single soil sample. The mismatch between the estimated SC and the experimental results suggested that the applicability of the proposed approach may be soil-dependent. Therefore, further research on various soil types is necessary.

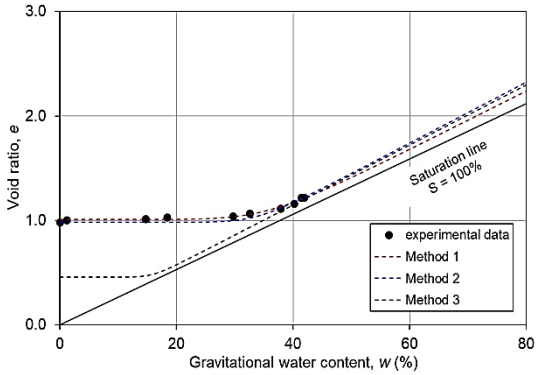

Figure 12. Shrinkage fitting curves from the three studied methods

3.3. SWCC of the soil

Figure 13 shows the measured gravimetric water content as a function of matric suction for the soil. When the *gev* for the soil was 4.49 kPa, and the residual suction was 305.98 kPa. When suction is lower than *gev*, the gravimetric water content remains almost constant at 41.84% as suction increases. As the suction increased from 4.49 kPa ~ 305.98 kPa, the gravimetric water content decreased rapidly to approximately 10%. Beyond the residual suction, from 305.98 kPa to 1000000 kPa, the gravimetric water gradually approached 0%. The *w*-SWCC parameters were a_{fx} of 14.546, n_{fx} of 1.226, and m_{fx} of 1.092.

The change in void ratio with suction was used to calculate the degree of saturation; therefore, the *S*-SWCC was obtained and presented in Fig. 14. The obtained air-entry value was 8.34 kPa (i.e., *AEV* = 8.34), which is approximately 2 times higher than the value observed from the *w*-SWCC. The result confirms that *w*-SWCC underestimates the soil's air-entry value. The consideration of volume change during the test also results in changes in the SWCC parameters a_{fx}, n_{fx}, and m_{fx}. A significant change in a_{fx} was observed, with its value increasing by nearly twofold to reach an a'_{fx} of 28.65 (Fig. 14). The slope of the SWCC did not vary appreciably, suggesting that the curve mainly experienced a horizontal shift toward the left along the suction axis.

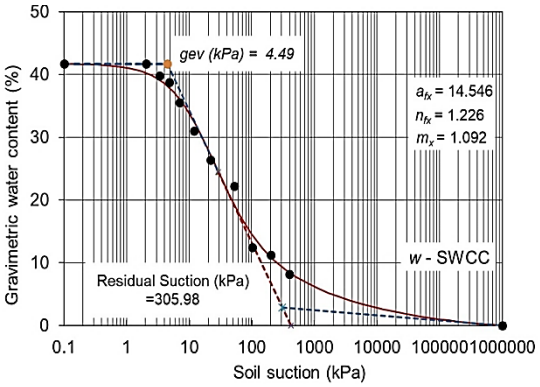

Figure 13. *w*-SWCC of the soil

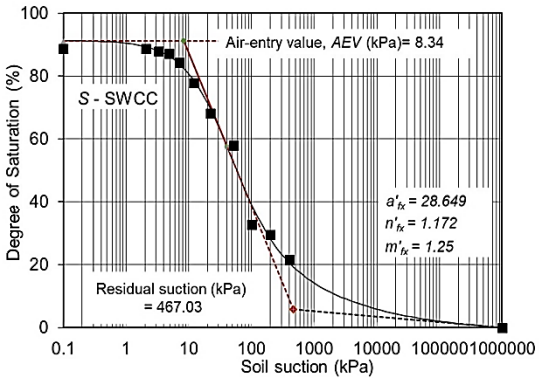

Figure 14. *S*-SWCC of the soil

3.4. Unsaturated shear strength and permeability functions

As the *S*-SWCC parameters used to predict the unsaturated shear strength of the soil, the shear strength envelope starts at *AEV* of 8.34 kPa. The maximum shear strength value at the residual suction is 83.99 kPa (Fig. 15), which is greater than that of the shear strength envelope constructed based on the *w*-SWCC

parameters (Fig. 16). When using the *w*-SWCC parameters, the unsaturated condition comes earlier with *gev* of 4.49 kPa. The whole shear strength curve goes under the curve predicted by *S*-SWCC at the same soil suction (Fig. 16). This implies that without considering the volume change in the SWCC, the shear strength of soil is underestimated as the SWCC predicts it.

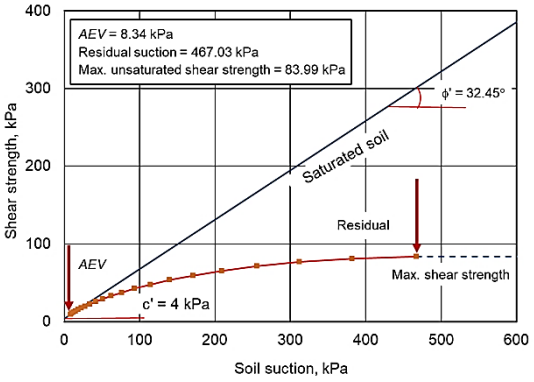

Figure 15. Shear strength envelope of the soil based on *S*-SWCC

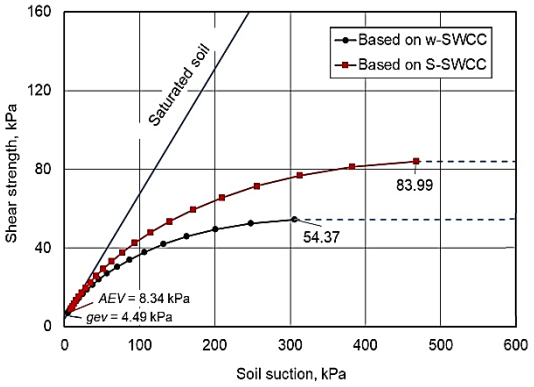

Figure 16. Changes in shear strength envelopes and maximum shear strength values for different types of SWCC

Figure 17 presents the predicted soil permeability using the *w*-SWCC and *S*-SWCC parameter sets. The permeability curve based on *w*-SWCC has lower values than those constructed from *S*-SWCC parameters under the same soil suction conditions. For example, at a suction of 467.03 kPa, the permeability based on *w*-SWCC is 1×10^{-5} m/s, which is five times lower than that based on *S*-SWCC (5×10^{-5} m/s). The permeability of soil under residual suction conditions shows a slight difference between the two SWCC types. However, the permeability derived from the *w*-SWCC (3.5×10^{-5} m/s) remains lower than that from the *S*-SWCC (5×10^{-5} m/s). It can be said that the *w*-SWCC parameter set overestimates soil permeability.

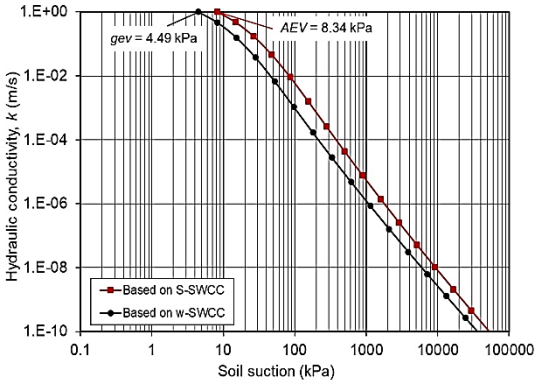

Figure 17. Changes in the permeability curve for different types of SWCC

The gaps in predicting the shear strength envelope and permeability curve arise from differences in air-entry values, which are influenced by the volume change accounted for in the SWCC.

4. Discussions

This study provides a procedure for best accounting for volume change effects in determining the air-entry value and the fitting parameters of the SWCC. The effects of volume change ultimately influence the calculation of unsaturated soil property functions. The volume change (defined by SC) is governed by the target initial void ratio or compaction degree of the soil specimen. The initial void ratio dictates the shift in the calculated air-entry values from the *w*-SWCC to the *S*-SWCC. An accurate estimate of the shift in the SWCC requires additional SC and experimental (or estimated) data.

This study showed that the SC curve and its fitting parameters can be combined with the empirical equations proposed by Fredlund (2000) and Wong et al. (2019) to provide a close fit to the experimental data. The results also show that estimates of the fitting parameters for the SC tests based on Atterberg limits cannot be used with confidence to estimate the *S*-SWCC and unsaturated soil property functions of the tested weathered soil. Nevertheless, as the conclusions are based on a single soil type, additional studies across various soil types are necessary before any general assessment of the method can be made.

It is noted that, in engineering practice, due diligence is not always exercised when assessing the true SWCC from the *S*-SWCC. Estimates of the air-entry value based strictly on the *w*-SWCC may lead to considerable errors in predicted results.

In this study, it was assumed that hysteresis effects between the drying and wetting curves were either negligible or could be estimated with sufficient confidence. The data and analysis focused on the drying-type curves. Further studies are recommended to determine the best way to accommodate the wetting curves. Additional studies are recommended to provide details on integrating the SC into the *w*-SWCC for *S*-SWCC calculation.

5. Conclusions

This study estimates methods to determine the SC without actual SC testing, examines the effects of compaction degree (i.e., target initial void ratio and dry density) on the SC, and underscores the importance of accounting for volume change when predicting the SWCC of the soil. This study is confined to a single type of weathered soil obtained from one natural slope. Accordingly, the conclusions apply to this particular soil and site condition. Within this defined scope, the main conclusions of the study are summarized as follows:

- SC constructed based on the Atterberg limits was not fully consistent with the experimental results for the studied weathered soil having *LL* of 26.35, *PL* of 19.05.

- The SC was significantly affected by the compaction degree (i.e., target initial void ratio and dry density). This is because the minimum void ratio, emin, increased sensitively with the target initial void ratio of the soil specimen.

- *SL* values were also affected by the compaction degree via the change in e_{min} and SC. The higher the compacted soil specimen, the lower the *SL* was obtained.

- The empirical equations for a_{sh} and b_{sh} suggested by Fredlund (2000) and for c_{sh} by Wong et al (2019) provide the most accurate SC parameter set for achieving the best fitting curve without experimental SC data.

- The air-entry value from the *S*-SWCC is more representative than that of the *w*-SWCC. The air-entry value obtained from the *S*-SWCC is much higher than the values obtained from the *w*-SWCC due to the consideration of the volume change.

- The air-entry value obtained from the *S*-SWCC predicts greater shear strength and higher permeability for the soil compared to the *w*-SWCC.

Acknowledgements

This research is funded by the Vietnam Ministry of Education and Training (MOET) under grant number B2025-DHH-06, and by the Natural Sciences and Engineering Research Council of Canada (NSERC), RGPIN 3787-2013, to the University of Saskatchewan, Saskatoon, for research into Implementation Techniques for Unsaturated Soil Mechanics.

References

ASTM-D2487, 2025. Standard Practice for Classification of Soils for Engineering Purposes (Unified Soil Classification System). ASTM International West Conshohocken, PA.

ASTM-D4318, 2017. Standard Test Methods for Liquid Limit, Plastic Limit, and Plasticity Index of Soils. ASTM International West Conshohocken, PA.

ASTM-D6836, 2016. Standard test methods for determination of the soil water characteristic curve for desorption using a hanging column, pressure extractor, chilled mirror hygrometer, and/or centrifuge. ASTM International West Conshohocken, PA.

ASTM-D6913, 2009. Standard Test Methods for Particle-Size Distribution (Gradation) of Soils Using Sieve Analysis. ASTM International West Conshohocken, PA.

Bao C.G., Gong B.-W., Zhan L.-T., 1998. Properties of unsaturated soils and slope stability of expansive soils. In Proceedings of the Second International Conference on Unsaturated Soils-UNSAT98, Beijing, China, 1, 71–98.

Brooks R.H., Corey A.T., 1964. Hydraulic Properties of Porus Media. Colorado State University Hydrology Paper, 3, 27.

Casagrande A., 1932. Research on the Atterberg limits of soils. Public roads, 13(8), 121–136.

Dao M.D., Vu C.M., Hoang H.Y., Nguyen T.L., Do M.D., 2023. Analysis of landslide kinematics integrating weather and geotechnical monitoring data at Tan Son slow moving landslide in Ha Giang province. Vietnam Journal of Earth Sciences, 45(2), 131–146. https://doi.org/10.15625/2615-9783/18204.

Fredlund D.G., 2019. Determination of unsaturated soil property functions for engineering practice. In 17th African Regional Conference on Soil Mechanics and Geotechnical Engineering, Cape Town South Africa.

Fredlund D.G., Xing A., 1994. Equations for the soil-water characteristic curve. Canadian Geotechnical Journal, 31(4), 521–532. Doi: 10.1139/t94-061.

Fredlund D.G., Rahardjo H., Fredlund M.D., 2012. Unsaturated Soil Mechanics in Engineering Practice. John Wiley & Sons.

Fredlund D.G., Vanapalli S.K., Xing A., Pufahl D.E., 1995. Predicting the shear strength function for unsaturated soils using the soil-water characteristic curve. In Proceedings of the first international conference on Unsaturated soils. UNSAT'95. Paris. France, 6-8 September 1995, 1, 63–69.

Fredlund D.G., Xing A., Huang S., 1994. Predicting the permeability function for unsaturated soils using the soil-water characteristic curve. Canadian Geotechnical Journal, 31(4), 533–546. https://doi.org/10.1139/t94-062.

Fredlund M.D., 2000. The role of unsaturated soil property functions in the practice of unsaturated soil mechanics. University of Saskatchewan. https://hdl.handle.net/10388/etd-10212004-002824.

Fredlund M.D., Wilson G.W., Fredlund D.G., 2002. Representation and estimation of the shrinkage curve. In Proc., 3rd Int. Conf. on Unsaturated Soils, UNSAT, 145–149.

Gardner W.R., 1958. Mathematics of isothermal water conduction in unsaturated soils. Highway research board special report, 40, 78–87.

Giráldez J.V., Sposito G., Delgado C., 1983. A general soil volume change equation: I. The two-parameter model. Soil Science Society of America Journal, 47(3), 419–422. https://doi.org/10.2136/sssaj1983.03615995004700030005x.

GSCT, 2022. GCTS Operating Instructions for SWC-050, Version 1.2, Tempe, Arizona, USA.

Haines W.B., 1923. The volume-changes associated with variations of water content in soil. The Journal of Agricultural Science, 13(3), 296–310. https://doi.org/10.1017/S0021859600003580.

Hai-Bang Ly, Hoang-Long Nguyen, Viet-Hung Phan, Vincent Monchiet, 2024. Hybrid approach for permeability prediction in porous media: combining FFT simulations with machine learning. Vietnam

Journal of Earth Sciences, 46(4), 515–532. https://doi.org/10.15625/2615-9783/21133.

Holtz R.D., Kovacs W.D., Sheahan T.C., 1981. An introduction to geotechnical engineering. Englewood Cliffs, NJ: Prentice-hall, vol. 733.

Khalili N., Khabbaz M.H., 1998. A unique relationship for χ for the determination of the shear strength of unsaturated soils. Géotechnique, 48(5), 681–687. Doi: 10.1680/geot.1998.48.5.681.

Leong E., Wijaya M., 2015. Universal soil shrinkage curve equation. Geoderma, 237–238, 78–87. https://doi.org/10.1016/j.geoderma.2014.08.012.

Peng X., Horn R., 2007. Anisotropic shrinkage and swelling of some organic and inorganic soils. European Journal of Soil Science, 58(1), 98–107. https://doi.org/10.1111/j.1365-2389.2006.00808.x.

Pham V.T., Luong L.H., Tran T.N., Nguyen Q.P., Phan T.T., Dinh T.Q., Dao M.D., Nguyen C.L., Nguyen H.C., 2023. Mechanism and numerical simulation of a rapid deep-seated landslide in Van Hoi reservoir, Vietnam. Vietnam Journal of Earth Sciences, 45(3), 357–373. https://doi.org/10.15625/2615-9783/18539.

Salih A.G., 2012. Review on granitic residual soils' geotechnical properties. Electronic Journal of Geotechnical Engineering, 17(3), 2645–2658.

Tariq A.U.R., Durnford D.S., 1993. Analytical volume change model for swelling clay soils. Soil science society of America journal, 57(5), 1183–1187. https://doi.org/10.2136/sssaj1993.03615995005700050003x.

Tran T.P.A., Chang I., Tran N.T., Cho G.-C., 2023a. Numerical modelling of slope stabilization with xathan gum-treated soil. Vietnam Journal of Earth Sciences, 45(1), 98–110. https://doi.org/10.15625/2615-9783/17924.

Tran T.P.A., Fredlund D.G., Nhan T.T., 2023c. Use of SWC-050 for Measuring Soil-Water Characteristic Curves. In International Conference on Geotechnics for Sustainable Infrastructure Development. Singapore: Springer Nature Singapore, 2425–2433.

Tran T.P.A., Fredlund D.G., Vanapalli S., 2023b. Anchor Conditions for Estimated Unsaturated Shear Strength Functions. Canadian Geotechnical Journal, 60(12), 1938–1953. https://doi.org/10.1139/cgj-2022-0255.

van Genuchten M.T., 1980. A closed-form equation for predicting the hydraulic conductivity of unsaturated soils. Soil Science Society of America Journal, 44(5), 892–898. https://doi.org/10.2136/sssaj1980.03615995004400050002x.

Vanapalli S.K., 2009. Shear strength of unsaturated soils and its applications in geotechnical engineering practice. In Keynote Address. Proc. 4th Asia-Pacific Conf. on Unsaturated Soils. New Castle, Australia, 579–598.

Vanapalli S.K., Oh W.-T., 2021. Analytical and numerical methods for prediction of the bearing capacity of shallow foundations in unsaturated soils. Soils and Rocks, 44. https://doi.org/10.28927/SR.2021.066521.

Vanapalli S.K., Fredlund D.G., Pufahl D.E., Clifton A.W., 1996. Model for the prediction of shear strength with respect to soil suction. Canadian Geotechnical Journal, 33(3), 379–392. Doi: 10.1139/t96-060.

Wijaya M., Leong E.C., 2016. Estimation of soil shrinkage curve. In Unsaturated Soil Mechanics - from Theory to Practice. Edited by E. Chen et al. Taylor & Francis Group, London, 785–789.

Wong J.M., Elwood D., Fredlund D.G., 2019. Use of a three-dimensional scanner for shrinkage curve tests. Canadian Geotechnical Journal, 56(4), 526–535. https://doi.org/10.1139/cgj-2017-0700.

Zhang L.L., Fredlund D.G., Fredlund M.D., Wilson G.W., 2014. Modeling the unsaturated soil zone in slope stability analysis. Canadian Geotechnical Journal, 51(12), 1384–1398. https://doi.org/10.1139/cgj-2013-0394.

APPENDIX

Table 1. Classification and physical properties of the soil

Classification and physical properties			**Values**		
			Case 1	**Case 2***	**Case 3**
Soil particles					
Sand		%		46.20	
Silt		%		49.10	
Clay		%		2.68	
At dry condition					
Target dry density	γ_{ct}	g/cm^3	1.36	1.20	1.10
Target initial void ratio	e_{ot}		0.95	1.22	1.41
Specific gravity	G_s			2.65	
After saturation process					
Gravimetric water content	w	%	31.56	41.84	42.88
Degree of saturation	S	%	87.86	91.25	80.42
Atterberg limit					
Liquid limit	LL	%		26.35	
Plastic limit	PL	%		19.05	
Plasticity index	PI	%		7.30	
*used to calculate the *S*-SWCC					

Table 2. SC parameters obtained from 3 methods

SC parameters	**Method 1**	**Method 2**	**Method 3**
$a_{sh} = e_{min}$	1.012	0.987	0.464
b_{sh}	0.362	0.339	0.160
c_{sh}	7.810	11.97	11.97
SL_{ash}	38.16	37.22	17.50